Automatic Three-Dimensional Multimodality Registration Using Radionuclide Transmission CT Attenuation Maps: A Phantom Study

Damini Dey, Piotr J. Slomka, Leszek J. Hahn and Reinhard Kloiber

Departments of Physics and Astronomy and Radiology, University of Calgary, Calgary; Division of Nuclear Medicine, Foothills Hospital, Calgary; and London Health Sciences Center, Victoria Campus, University of Western Ontario, London, Ontario, Canada

Coregistration of images from a single subject, acquired by different modalities, is important in clinical diagnosis, surgery and therapy planning. The purpose of this study was to evaluate, using a physical torso phantom, a novel, fully automated method for three-dimensional image registration of CT and SPECT, using radionuclide transmission (RNT) attenuation maps. **Methods:** We obtained CT scans and SPECT scans paired with RNT maps of an anthropomorphic cardiac phantom. RNT attenuation maps were acquired using an uncollimated ^{99m}Tc-filled flood source. RNT and SPECT scans were acquired in the same spatial orientation (usual clinical practice in nonuniform attenuation correction). In addition, CT attenuation maps (CTMAPs) for ^{99m}Tc SPECT were generated from CT by linear energy scaling. RNT maps were registered to CT and CTMAPs by iterative simplex minimization of count difference and uniformity index (sum of RNT map intensity variances corresponding to each intensity level in the CT volume). In each iteration, three shifts and three angles were adjusted. To register SPECT to CT, we applied the RNT transformation parameters to SPECT. **Results:** RNT maps could be registered to CT and CTMAP images using both criteria. The average three-dimensional distance between landmark and automated registration was 2.5 ± 1.2 mm for count difference and 3.3 ± 1.3 mm for uniformity index. The three-dimensional reproducibility errors were 1.2 ± 0.7 mm for count difference, 2.1 ± 0.5 mm for uniformity index and 2.3 ± 1.0 mm for manual marker registration. The minimization of uniformity index was robust when up to 50% CT or RNT slices were missing and was not affected significantly (<2 mm) by realistic variation in CT values (±12 Hounsfield units). **Conclusion:** In addition to typical use in nonuniform attenuation correction, RNT maps can be used for fully automated three-dimensional registration of SPECT to CT. Such registration is not affected by features and quality of SPECT images and avoids difficulties associated with fiducial markers. Our method can be applied to SPECT-CT registration of various organs, such as brain, heart, lungs, breasts and abdomen, including oncological scans.

Key Words: coregistration; automated image registration; transmission attenuation maps

J Nucl Med 1999; 40:448–455

Correlative registration of images obtained from a single subject using different modalities (e.g., SPECT and CT or SPECT and MRI) is increasingly useful in both research and patient care (*1*). Accurate mapping of data between different imaging modalities into common data coordinates may be required for clinical diagnosis, surgery or therapy planning, and detection of anatomic or functional changes from previous scans. Accurate anatomic localization of abnormalities in functional SPECT (or PET) images is critical, yet the images may have few anatomic landmarks or may differ substantially from anatomic CT or MR images.

Although most of the published articles on multimodality image registration have been mainly devoted to brain imaging (*2–5*), a few multimodality image fusions have been reported in other anatomic regions, such as chest, abdomen and pelvis (*6–8*). A large number of the proposed image registration algorithms use external markers or a combination of external markers and anatomic landmarks. Use of such markers or stereotactic frames can complicate acquisition protocols and may not be clinically feasible. In addition, external markers can be used for the brain but not for the thoraco-abdominal region, because variable displacement of the skin relative to internal organs adversely affects image registration (*6*). Most automatic approaches are specific to a particular type of SPECT scan, and no single method works well on all image datasets (*1*). For the thorax and abdomen, in particular, there is a great need for robust automatic image registration methods, but few have been proposed (*6*).

This article presents a fully automated method for registering three-dimensional CT and SPECT images, using radionuclide transmission (RNT) attenuation maps. This method is not specific to a particular type of SPECT scan and does not require external markers. RNT attenuation maps, in the same spatial orientation as SPECT, can now be acquired routinely with instrumentation for nonuniform attenuation correction (used mainly for cardiac SPECT imaging). This study indicates that, in addition to nonuniform attenuation correction, RNT attenuation maps can be applied to register SPECT images to CT using automatic registration methods. This article presents preliminary results with an anthropomorphic cardiac phantom only, but transmission attenuation maps

Received Jan. 20, 1998; revision accepted Aug. 4, 1998.

For correspondence or reprints contact: Piotr J. Slomka, PhD, Department of Nuclear Medicine, London Health Sciences Center, 75 South St., London, Ontario, Canada N6A 4G5.

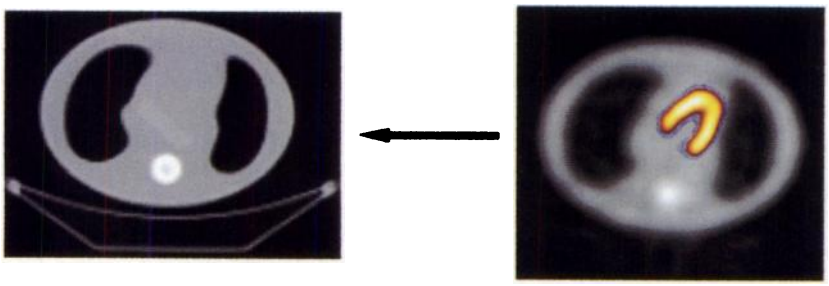

FIGURE 1. Method for automatic SPECT-CT registration for anthropomorphic cardiac phantom using radionuclide transmission (RNT) attenuation maps. RNT attenuation maps were acquired in same orientation as SPECT (usual clinical practice in non-uniform attenuation correction). RNT maps were registered to CT using automatic three-dimensional voxel-based registration. Transformation parameters obtained were applied to SPECT.

can potentially be applied to automatic multimodality image registration for SPECT scans of the brain, heart, lungs, breasts and abdomen, including oncological scans.

MATERIALS AND METHODS

Image Acquisition

We obtained CT and SPECT scans paired with RNT attenuation maps of an anthropomorphic cardiac phantom with lung, cardiac and spine inserts (Data Spectrum Corporation, Hillsborough, NC). CT images were acquired on a Hi-speed CT scanner (General Electric, Milwaukee, WI), using a peak voltage of 120 kV, 512 × 512 matrix, pixel size 0.94 mm/pixel and contiguous slices with slice thickness of 5 mm.

For SPECT acquisition, 660 mCi (24,420 MBq) ^{99m}Tc were placed in the myocardial insert. No background activity was placed in the phantom. SPECT acquisition was performed using a single-head Genesys gamma camera (ADAC, Milpitas, CA). The following acquisition parameters were used: 128 × 128 matrix, 120 stops over 360°, 15 s per stop and pixel size of 4.73 mm. After SPECT acquisition, radioactivity in the phantom was allowed to decay over 48 h. RNT images in the same orientation as SPECT were then obtained with an uncollimated ^{99m}Tc flood source and the collimated single-head Genesys gamma camera. The flood source was filled with 20 mCi (740 MBq) ^{99m}Tc and taped to the counterbalance of the gamma camera, opposite the head. The acquisition parameters were 128 × 128 matrix, 120 stops over 360°, 15 s per stop and pixel size of 4.73 mm.

Image Preprocessing

RNT maps were registered to both original CT images in Hounsfield units and to CT attenuation maps (CTMAPs) corresponding to 140 keV. To convert CT images to attenuation maps for 140 keV, the linear attenuation coefficient of water (μ_{cr}) corresponding to the effective energy of the CT scanner (E_{CT}) was calculated. By experimentally measuring the half-value layer for water at 120 kVp, μ_{cr} was found to be 0.165 cm^{-1}.

CT images were converted to attenuation maps corresponding to the photon energy of 140 keV by linearly scaling with the ratio of μ_{cr} to the known narrow beam linear attenuation coefficient of water at 140 keV (0.153 cm^{-1}) (linear energy translation [*9*]. The images were then rebinned from 512 × 512 to 128 × 128 matrix.

The measured RNT projections were converted to integrals of linear attenuation coefficients (*10*):

$$\mu(x, y, t) = [\ln(N_o)(x, y, t)/RNT(x, y, t))]/x_o, \qquad \text{Eq. 1}$$

where $N_0(x, y, t)$ = blank scan projection value at position x,y and projection angle t; $RNT(x, y, t)$ = transmission projection value at position x,y and projection angle t, and x_0 = pixel size in centimeters.

These projections were reconstructed by filtered backprojection with ramp filter and filtered by a three-dimensional postreconstruction Butterworth filter. A frequency cutoff of 0.41 cycles/cm and order 5 was used. Because of scatter, the linear attenuation coefficients thus obtained do not correspond to narrow-beam attenuation coefficients. The mean counts corresponding to water in the phantom were determined by region-of-interest (ROI) analysis. The RNT images were then scaled by a factor such that the mean counts corresponding to water were equal to the narrow-beam linear attenuation coefficient for water at 140 keV (0.153 cm^{-1}).

SPECT images were corrected for scatter using a dual-energy window subtraction technique (*11*). The scatter fraction used was

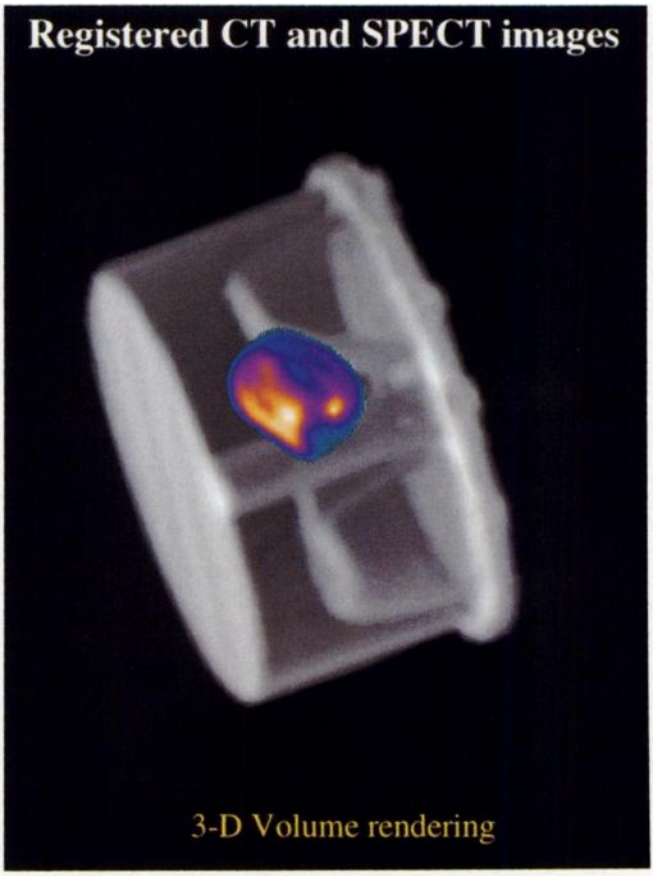

FIGURE 2. Registered CT and SPECT images of anthropomorphic cardiac phantom (three-dimensional volume rendering).

0.5. CTMAPs were registered to the SPECT images by automatic volume registration, using RNT maps. Scatter-corrected SPECT projections were reconstructed with an ordered subsets expectation maximization (OSEM) algorithm (*12*) with attenuation correction, using the registered CTMAP. For the OSEM reconstruction, 15 subsets were used, with 8 projections in each subset and 4 iterations.

Automatic Volume Registration

Figure 1 shows the SPECT-CT image registration technique. The steps for automatic SPECT-CT registration are as follows:

1. SPECT and RNT maps acquired in same orientation (usual clinical practice in non-uniform attenuation correction.
2. Register RNT maps to CT using automated three-dimensional voxel-based registration.
3. Apply RNT transformation parameters to SPECT.

All image registrations were made using multimodality software on a Pentium Pro 200 MHz workstation (Hermes; Nuclear Diagnostics, Stockholm, Sweden) (*13*). All automatic image registrations were three-dimensional volume registrations and were performed in two steps. First, an approximate image alignment was made using a technique based on principal-axes transformation (*14*). Then a simplex minimization algorithm (*15*) was applied to the initial principal-axes transformed image by independently adjusting six transformation parameters: X shift, Y shift, Z shift, XY tilt, XZ tilt and YZ tilt. Because the pixel sizes were known, scaling in X, Y and Z was constrained for all registrations.

We registered each set of images twice, using simplex minimization of two convergence criteria: count difference (*16*) and uniformity index. Count difference is defined as the sum of the differences between the voxel values of the volumes to be registered. Uniformity index, similar to the criterion used by Woods et al. (*3*), is defined as the sum of the voxel variances on the RNT image corresponding to each voxel intensity for the CT image. Our method differs from the method used by Woods et al. (3) in the minimization technique, because we used simplex minimization (*15*). The result of each image registration was visually assessed simultaneously on all image slices in different orientations. Two visual presentation techniques were used to verify registered image accuracy: a roving window display technique and overlay of the registered image and the image to which it is to be registered (*16*).

Experiments

To evaluate this registration technique, we performed the following sets of experiments.

Comparison of Automatic Volume Registration with Manual Landmark-Based Registration Method. Automated volume registration using count difference and uniformity index criteria were compared to the commonly used method of registration using markers.

A set of nine landmarks was selected on the anthropomorphic cardiac phantom. Eight were plastic screws at various positions. The remaining landmark was the end of the spine insert. RNT images were registered to CTMAPs using these landmarks. The registered RNT images were then misaligned six times using various combinations of shifts and rotations; the angles were changed from −6° to 6° and the shifts between −8 and 8 pixels (−30 to 30 mm). These were realistic misalignments. The misaligned images were re-registered using landmarks.

RNT images were registered to CTMAPs using simplex minimization of count difference. The registered RNT images were misaligned six times using the same combinations of position and tilt parameters as for landmark registration. The angles were changed from −6° to 6° and the shifts between −8 and 8 pixels (−30 to 30 mm). Each set of images was re-registered using simplex minimization of count difference.

RNT images were registered to CTMAP using simplex minimization of uniformity index. The registered RNT images were misaligned six times using the same combinations of position and tilt parameters as for landmark registration. The angles were changed from −6° to 6° and the shifts between −8 and 8 pixels (−30 to 30 mm). Each set of images was re-registered using simplex minimization of uniformity index.

In total, 18 registrations were performed, 6 for each method. For each misalignment test, the same shifts and rotation parameters were used.

Three-Dimensional Difference from Marker Registration. For each of the six misalignment tests, the shifts and angles for each image registration method (landmark, automated volume registration using count difference and uniformity index) differ slightly from one another. For count difference and uniformity index, differences in all six transformation parameters from marker registration were calculated. Three-dimensional difference from marker registration was defined as the three-dimensional distance in millimeters corresponding to these differences in the six transformation parameters. The method used to calculate the three-dimensional distance is described in equations 2–5.

For each misalignment test, three-dimensional difference from marker registration for count difference and uniformity index was calculated for five anatomic markers at different positions in the phantom. The average three-dimensional differences from marker registration were calculated for count difference and uniformity index.

Three-Dimensional Registration Reproducibility Error. For landmark registration, count difference and uniformity index, we assessed registration reproducibility in the following way. For each misalignment test, the transformation parameters obtained after re-registration differ very slightly from the shifts and tilts used to misalign the RNT images. Three-dimensional registration reproducibility error was defined as the three-dimensional distance in millimeters corresponding to these small residual errors in all six transformation parameters (*17*). The method used to calculate the three-dimensional distance corresponding to the errors in the six transformation parameters is described in equations 2–5.

For each of the 18 misalignment tests corresponding to the three registration methods, three-dimensional registration reproducibility error was calculated for five anatomic markers at different positions in the phantom. For each registration method, the average three-dimensional registration reproducibility errors were calculated.

Three-Dimensional Distance Calculation. For each anatomic marker point P, at position (x, y, z), by introducing a fourth coordinate w, homogeneous coordinates (x_h, y_h, z_h, w) can be defined. The conversion between Cartesian (x, y, z) and homogeneous coordinates is given by:

$$x = \frac{x_h}{w}, y = \frac{y_h}{w}, z = \frac{z_h}{w}. \quad \text{Eq. 2}$$

For example, for the point P, the homogeneous coordinates are:

$$x_h = x, y_h = y, z_h = z, w = 1. \quad \text{Eq. 3}$$

Because of the errors in shifts and angles, the point P can be transformed into another point P' with Cartesian coordinates (x', y', z') and homogeneous coordinates (x_h', y_h', z_h', w'). This transformation is given by a 4 × 4 transformation matrix:

$$\begin{bmatrix} x_h' \\ y_h' \\ z_h' \\ w' \end{bmatrix} = \begin{bmatrix} r_{11} & r_{12} & r_{13} & t_x \\ r_{21} & r_{22} & r_{23} & t_y \\ r_{31} & r_{32} & r_{33} & t_z \\ 0 & 0 & 0 & 1 \end{bmatrix} \begin{bmatrix} x_h \\ y_h \\ z_h \\ w \end{bmatrix}, \quad \text{Eq. 4}$$

where the matrix elements r_{11} to r_{33} are the rotational components, derived from the errors in the XY, XZ and YZ angles (*18*); and the t_x, t_y and t_z elements correspond to the errors in X, Y and Z shifts (translation). The three-dimensional distance in millimeters corresponding to this transformation, r, is simply:

$$r = \sqrt{(x' - x)^2 + (y' - y)^2 + (z' - z)^2}. \quad \text{Eq. 5}$$

RNT-CT Registration Reproducibility. RNT images were registered to the original CT images (in Hounsfield units) using simplex minimization of count difference and uniformity index. For each convergence criterion, the registered RNT images were misaligned using six different combinations of position and tilt parameters. The angles were changed from −6° to 6° and the shifts between −8 and 8 pixels (−30 to 30 mm). Each set of images was then re-registered using automatic volume registration. As in RNT-CTMAP registration, for each convergence criterion, three-dimensional registration reproducibility errors for five anatomic markers were evaluated, and the average three-dimensional registration reproducibility error was calculated.

Effect of Missing Slices on RNT-CT Registration. To assess the effect of missing slices on RNT-CT registration, six pairs of CT and RNT images were created by removing slices from the top and bottom. The percentage of slices missing varied from 9% to 53%. If an upper limit >54% is used, the heart becomes truncated in the z (interslice) direction, which is not desirable. The truncated images were registered using simplex minimization of uniformity index.

Because of the missing slices, the transformation parameters differ from the transformation parameters corresponding to the untruncated data. We defined three-dimensional registration error as the three-dimensional distance in millimeters corresponding to these differences in the transformation parameters. For each registration, three-dimensional registration errors for five anatomic markers were evaluated, and the average three-dimensional registration error was calculated.

Effect of Variability in CT Voxel Values on RNT-CT Registration. To assess the effect of variability of CT voxel values on RNT-CT registration, 12 CT images were generated by varying the original CT voxel values in steps of 2 Hounsfield units (realistic variations). The resulting CT and RNT images were registered using simplex minimization of uniformity index.

Because of the variation in CT voxel values, the transformation parameters differ from those corresponding to the original CT data. We defined three-dimensional registration error as the three-dimensional distance in millimeters corresponding to these differences in the transformation parameters. For each registration, three-dimensional registration errors for five anatomic markers were evaluated, and the average registration error calculated.

For all experiments, the result of each image registration was visually assessed simultaneously on all image slices in different orientations using roving window display and image overlay techniques.

RESULTS

Figure 1 shows our automatic SPECT-CT registration technique using RNT attenuation maps. Figure 2 shows volume-rendered CT and SPECT images registered by this technique.

Comparison of Automatic Volume Registration with Manual Landmark-Based Image Registration

Figure 3 shows transverse slices of unregistered SPECT images overlaid on CT images. Figure 4 shows transverse slices of landmark-registered SPECT images overlaid on CT images. Figure 5 shows transverse slices of SPECT images, registered using count difference, overlaid on CT images. Figure 6 shows transverse slices of SPECT images, registered using uniformity index, overlaid on CT images. From visual assessment, CTMAP and RNT images could be registered successfully using automatic volume registration with count difference and uniformity index as well as manual landmark-based image registration.

For automatic volume registration using count difference, the average number of iterations was 96; each iteration took about 3.7 s. Therefore the total calculation time for each registration was about 6.0 min. For uniformity index, the average number of iterations was 94; each iteration took about 2.7 s. Therefore the total calculation time for each registration was about 4.0 min. For manual landmark-based registration, the typical time to register the images was about 10 min; most of this time was spent in manually identifying and marking the landmarks. Both CTMAP and RNT images were in 128 × 128 matrix.

For the three image registration methods (landmark-based image registration and automatic volume registration with count difference and with uniformity index), there were small differences in the transformation parameters for each misalignment test. These small differences could not be detected visually (Figs. 4–6). Table 1 shows three-dimensional difference from marker registration for automatic volume registration with count difference and uniformity index.

The results of the assessment of registration reproducibility for manual landmark-based registration, automatic volume registration using count difference and uniformity index are shown in Tables 2 and 3. Table 2 shows the error in transformation parameters and Table 3 the three-dimensional registration reproducibility error. Table 3 shows that the registration reproducibility of the automatic and manual image registration methods are comparable. All three values are within 1 SD of one another.

Tables 1 and 3 show that the three-dimensional differences from marker registration for both count difference and uniformity index are less than 3.5 mm and within 1 SD of

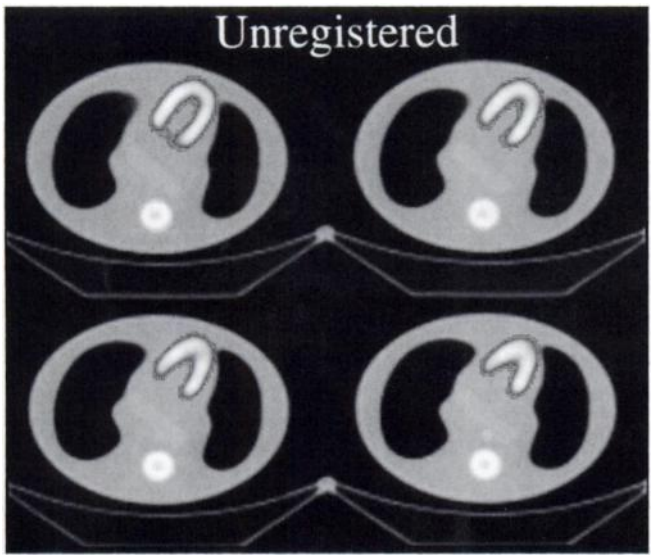

FIGURE 3. Transverse slices of unregistered SPECT images overlaid on CT images.

reproducibility error for marker registration (2.3 ± 1.0 mm). For the cardiac phantom, therefore, automatic volume registration with count difference and uniformity index is comparable to manual landmark-based registration.

RNT-CT Registration Reproducibility

RNT images could be successfully registered to CT images (in Hounsfield units) using count difference and uniformity index. For RNT-CT registration using count difference, the average number of iterations was 120, and the time per iteration was 3.9 s. The total time per registration was therefore 7.8 min. For uniformity index, the average number of iterations was 96; each iteration took about 2.7 s. Therefore the total time for each registration was about 4.3 min. The matrix sizes for RNT and CT images were 128 × 128 and 512 × 512, respectively. For RNT-CT registration using simplex minimization of count difference, the three-dimensional registration reproducibility error was 1.0 ±

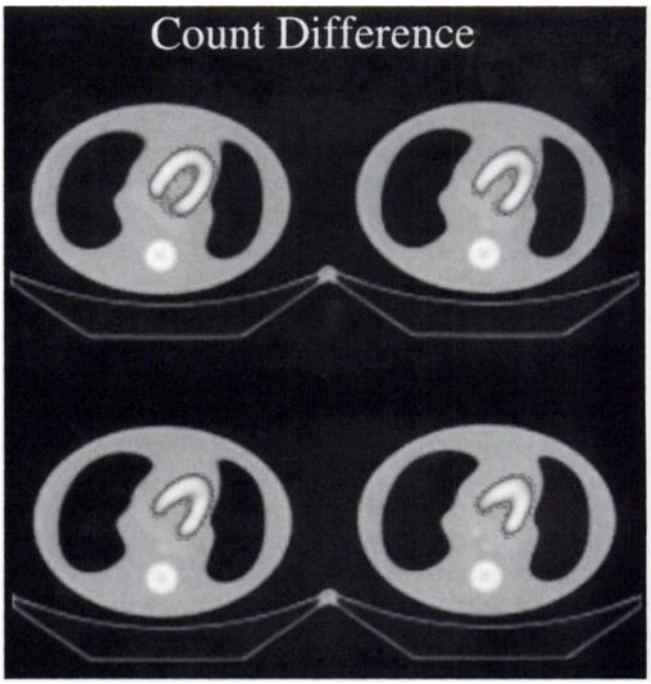

FIGURE 5. Transverse slices of SPECT images, registered using count difference, overlaid on CT images.

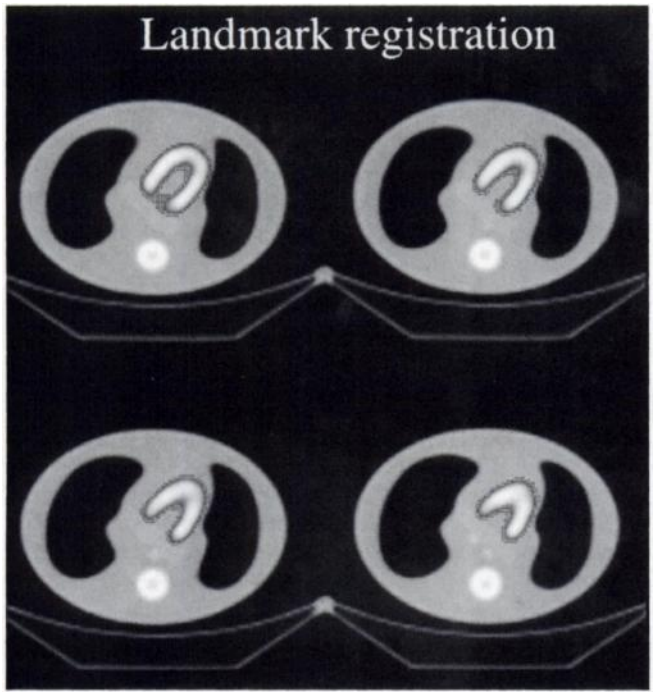

FIGURE 4. Transverse slices of landmark-registered SPECT images overlaid on CT images.

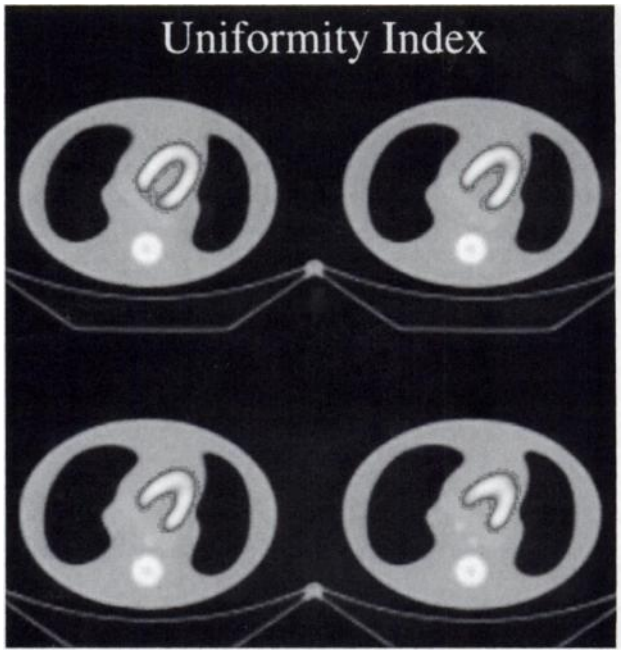

FIGURE 6. Transverse slices of SPECT images, registered using uniformity index, overlaid on CT images.

TABLE 1
Three-Dimensional Difference from Marker Registration for Automatic Volume Registration with Count Difference and Uniformity Index

	Three-dimensional difference from marker registration (mm)
Count difference	2.5 ± 1.2
Uniformity index	3.3 ± 1.3

Values are mean ± SD.

0.6 mm. For uniformity index, the three-dimensional registration reproducibility error was 2.0 ± 0.3 mm.

Effect of Missing Slices on RNT-CT Registration

From visual assessment, for each pair of truncated RNT-CT images, automatic volume registration using uniformity index was found to register the images successfully. Figure 7 shows the effect of missing slices on RNT-CT registration. Figure 7 shows that the registration error remained relatively stable and at less than 5 mm for up to 54% of slices missing from both volumes. If more than 54% of slices were missing from the volumes, the heart became truncated in the interslice direction.

Effect of Variability in CT Voxel Values on RNT-CT Registration

From visual assessment, for each CT image with altered CT voxel values, automatic volume registration using uniformity index was found to be successful. Figure 8 shows the effect of variation in CT voxel values on RNT-CT registration. For differences in CT voxel values of ±12 Hounsfield units in Figure 8, the registration error is less than 2 mm. These errors are comparable to the three-dimensional registration reproducibility error for RNT-CT image registration (2.0 mm).

TABLE 2
Registration Reproducibility for Manual Landmark-Based Registration, Automatic Volume Registration Using Count Difference and Uniformity Index: Error in Transformation Parameters

Transformation parameters	Count difference (n = 6)	Uniformity index (n = 6)	Manual landmark-based registration (n = 6)
X shift (mm)	0.4 ± 0.1	0.4 ± 0.2	1.3 ± 0.8
Y shift (mm)	0.4 ± 0.3	0.3 ± 0.3	1.5 ± 0.9
Z shift (mm)	0.2 ± 0.3	1.7 ± 0.3	0.2 ± 0.2
XY tilt (degrees)	0.3 ± 0.2	0.5 ± 0.3	0.2 ± 0.2
XZ tilt (degrees)	0.1 ± 0.1	0.2 ± 0.1	0.2 ± 0.1
YZ tilt (degrees)	0.7 ± 0.3	0.2 ± 0.1	0.2 ± 0.1

Values are mean ± SD.

TABLE 3
Three-Dimensional Registration Reproducibility Error for Automatic Volume Registration Using Count Difference and Uniformity Index and Manual Landmark-Based Registration

Image registration method	Three-dimensional registration reproducibility error (mm)
Count difference	1.1 ± 0.6
Uniformity index	2.1 ± 0.5
Manual landmark-based method	2.3 ± 1.0

Values are mean ± SD.

DISCUSSION

Comparison of Automatic Volume Registration with Manual Landmark-Based Image Registration

From our results, automatic volume registration using count difference and uniformity index are comparable to manual landmark-based image registration. The three-dimensional registration reproducibility error for all three registration methods is comparable, and the three-dimensional differences from marker registration for both count difference and uniformity index are less than 3.5 mm. The average times required to register the images using both count difference and uniformity index are less than those using landmark registration. Automatic volume registration

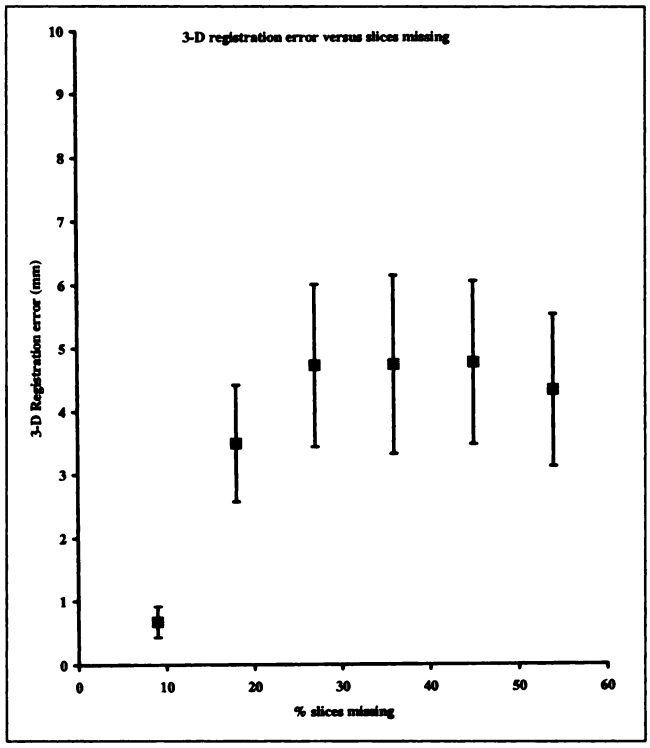

FIGURE 7. Plot of three-dimensional registration error (mm) versus slices missing. Slices were removed from top and bottom for both RNT and CT images.

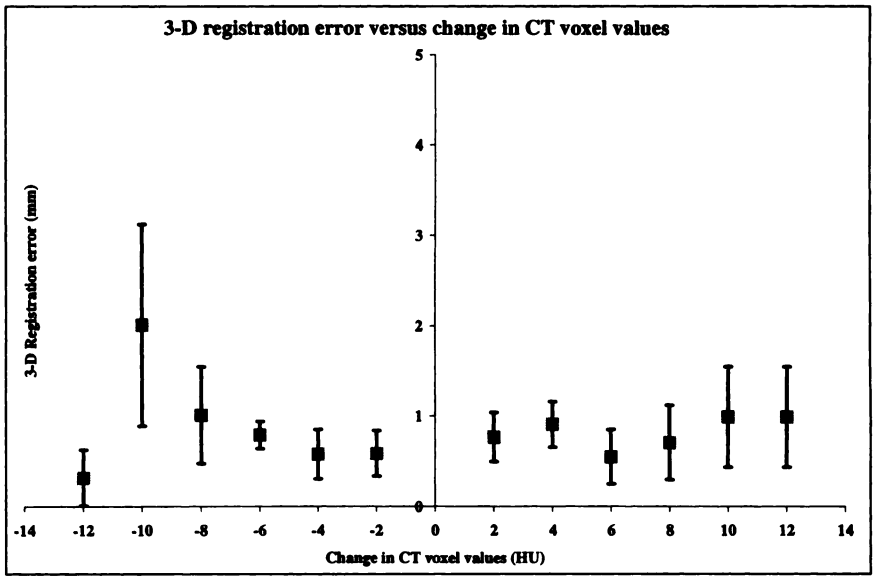

FIGURE 8. Plot of three-dimensional registration error versus change in CT voxel values.

requires no operator intervention and avoids difficulties associated with fiducial markers.

RNT-CT Registration

The results indicate that RNT maps can be successfully registered to CT images (in Hounsfield units) using simplex minimization of count difference and uniformity index. This is the first known application of both algorithms to co-registration of RNT attenuation maps and CT images. Count difference has been previously applied for registering patient images from the same modality (*16,19*). Woods' algorithm, however, is a more general algorithm and has been applied successfully for registering images from different modalities (e.g., for MR-PET images [*3*] and MR-SPECT images of the brain [*17*]). Because Woods' algorithm was validated for MRI-PET registration, we can speculate that for registering RNT maps to MR images, uniformity index may perform better than count difference. We found that uniformity index also provides better convergence than count difference.

Application of Our Method and Future Work

For most SPECT scans, there are no automated algorithms that can be applied for multimodality image registration; instead, external markers, or a combination of external markers and anatomic landmarks, must be used. Use of external markers or stereotactic frames is often not clinically feasible. For SPECT imaging in the thorax and abdomen, even external markers are not appropriate, because variable displacement of the markers from internal organs affects image registration (*6*).

In this article, we described a method for automated SPECT-CT image registration using RNT attenuation maps. Although we acquired RNT attenuation maps sequentially using an uncollimated flood source, for most current gamma cameras RNT attenuation maps can be acquired simultaneously with SPECT. Therefore, acquiring the RNT maps does not increase patient imaging time significantly. The method is clinically feasible and can be implemented easily. Because the registration method is not affected by features and quality of SPECT images, it can potentially be applied for automatic multimodality registration for SPECT scans of the brain, heart, lungs, breasts and abdomen.

Our method potentially could be applicable to SPECT-CT registration of oncological scans, in which accurate anatomic localization of the tumor can aid clinical diagnosis and treatment. As mentioned earlier, even external markers are not appropriate for oncological scans in the thorax and abdomen, because of variable displacement of external markers from internal organs.

Our method also has the potential to be applied to SPECT imaging using newer agents targeting specific brain functions, for example, dopamine D2-receptor imaging using ^{123}I-labeled pharmaceuticals (*20,21*). Because these images lack any anatomic information, accurate anatomic localization of the SPECT images is critical. We are currently investigating the application of this technique to patient data.

In addition to multimodality image registration for a single subject, transmission attenuation maps can also be used for intersubject registration of SPECT images, which is useful for comparing serial SPECT scans and for quantitative SPECT analysis. A common technique for quantifying cardiac and brain SPECT images is to compare each SPECT scan, on a voxel-by-voxel basis, to a database of normal patient studies (*16,17,19*). To perform voxel-by-voxel comparisons, it must be possible to accurately map patient images to common data coordinates. In a previous study (*22*), we used RNT images to register SPECT images of an anthropomorphic cardiac phantom simulating different patient situations. Because anatomic RNT images are not influenced by abnormal physiology, they are more suitable for intersubject and intrasubject registration than SPECT images. Transmission attenuation maps have been used for intersubject registration of cardiac PET images (*23,24*).

CONCLUSION

We have described an automated, clinically feasible method for SPECT-CT image registration using RNT attenuation maps. Such registration is not affected by features and quality of SPECT images and avoids difficulties associated with fiducial markers. The technique described in this preliminary phantom study can potentially be extended to SPECT imaging of the brain, lungs, heart, breasts and abdomen, including oncological scans.

ACKNOWLEDGMENTS

We thank Dr. Anna Celler, Vancouver General Hospital, for extensive use of the anthropomorphic phantom; Nuclear Diagnostics, Sweden for use of Hermes software and for use of a Pentium Pro 200 MHz workstation; and Dr. Ian Cunningham for useful discussions regarding the CT data.

REFERENCES

1. Weber DA, Ivanovic M. Correlative image registration. *Semin Nucl Med.* 1994;24:311–323.
2. Pelizzari CA, Chen GTY, Spelbring DR, Weichselbaum RR, Chen CT. Accurate three-dimensional registration of CT, PET, and/or MR images of the brain. *J Comput Assist Tomogr.* 1989;13:20–26.
3. Woods RP, Mazziotta JC, Cherry SR. MRI-PET registration with automated algorithm. *J Comput Assist Tomogr.* 1993;17:536–546.
4. Henri CJ, Collins DL, Peters TM. Multimodality image integration for stereotactic surgical planning. *Med Phys.* 1991;18:167–177.
5. Pohjonen H, Nikkinen P, Sipila O, et al. Registration and display of brain SPECT and MRI using external markers. *Neuroradiology.* 1996;38:108–114.
6. Pereault C, Schvartz C, Wampach H, et al. Thoracic and abdominal SPECT-CT image fusion without external markers in endocrine carcinoma. *J Nucl Med.* 1997;38:1234–1242.
7. Yu JN, Fahey FH, Gage HD, et al. Intermodality retrospective image registration in the thorax. *J Nucl Med.* 1995;36:2333–2338.
8. Kramer EL, Noz ME, Sanger JJ, Megibow AJ, Maguire GQ. CT-SPECT fusion to correlate radiolabeled monoclonal antibody uptake with abdominal CT findings. *Radiology.* 1989;172:862–865.
9. LaCroix K, Tsui BMW, Hasegawa BH, et al. Investigation of the use of x-ray CT images for attenuation compensation in SPECT. *IEEE Trans Nucl Sci.* 1994;41: 2793–2799.
10. King MA, Tsui BMW, Pan TS. Attenuation compensation for cardiac single-photon emission computed tomographic imaging. Part 1. Impact of attenuation and methods of estimating attenuation maps. *J Nucl Cardiol.* 1995;2:513–524.
11. Jaszczak RJ, Greer KL, Floyd CE, et al. Improved SPECT quantification using compensation for scattered photons. *J Nucl Med.* 1984; 25:893–900.
12. Hudson HM and Larkin RS. Accelerated image reconstruction using ordered subsets of projection data. *IEEE Trans Med Imaging.* 1994;13:601–609.
13. Slomka PJ, Hurwitz GA, Stephenson J, et al. A volume-based image registration toolkit for automated comparison of paired nuclear medicine images [abstract]. *Med Phys.* 1995;22:1017.
14. Alpert NM, Bradshaw JF, Kennedy D, et al. The principal axes transform: a method for image registration. *J Nucl Med.* 1990;31:626–633.
15. Press WH, Teukolsky SA, Vetterling WT, et al. *Numerical Recipes in C.* 2nd ed. New York, NY: Cambridge University Press; 1992:408–412.
16. Slomka PJ, Hurwitz GA, Stephenson J, et al. Automated alignment and sizing of myocardial stress and rest scans to three-dimensional normal templates using an image registration algorithm. *J Nucl Med.* 1995;36:1115–1122.
17. Radau PE, Slomka PJ, Julin P, Hurwitz GA. Automated alignment and quantitative analysis of brain studies utilizing the clinical software BRASS [abstract]. *Eur J Nucl Med.* 1997;24:900.
18. Fosner, R. *Open GL Programming for Windows 95 and Windows NT.* Berkeley, CA: Addison-Wesley Developers Press; 1997:71–82.
19. Slomka PJ, Hurwitz GA, St. Clement G, et al. Three-dimensional demarcation of perfusion zones corresponding to specific coronary arteries: application for automated interpretation of myocardial SPECT. *J Nucl Med.* 1995;36:2120–2126.
20. Ichise M, Ballinger JR, Vines D, et al. Simplified quantification and reproducibility studies of dopamine D2-receptor binding with iodine-123-IBF SPECT in healthy subjects. *J Nucl Med.* 1997;38:31–37.
21. Tihonen J, Kuikka J, Bergstrom K, et al. Altered striatal dopamine re-uptake site densities in habitually violent and non-violent alcoholics. *Nature Med.* 1995;1:654–657.
22. Dey D, Hahn LJ, Slomka PJ, Kloiber RK. Comparison of precise and imprecise attenuation maps in quantitative cardiac SPECT [abstract]. *J Nucl Med.* 1997;38: 217P.
23. Pallotta S, Gillardi MC, Bettinardi V, et al. Application of a surface matching image registration technique to the correlation of cardiac studies in positron emission tomography by transmission images. *Phys Med Biol.* 1995;40:1695–1708.
24. Bacharach SL, Douglas MA, Carson RE, et al. Three-dimensional registration of cardiac positron emission tomography attenuation scans. *J Nucl Med.* 1993; 34:311–321.